Published in final edited form as:

J Nucl Cardiol. 2020 October ; 27(5): 1547–1562. doi:10.1007/s12350-018-1429-y.

Multiparametric assessment of left atrial remodeling using ^{18}F-FDG PET/CT cardiac imaging: A pilot study

Michael Ghannam, MD[a], **Hong Jun Yun, MD**[a], **Edward P. Ficaro, PhD**[b,c], **Hamid Ghanbari, MD, MPH**[a], **John J. Lazarus, MD, PhD**[a], **Matthew Konerman, MD**[a], **Ravi V. Shah, MD**[d], **Richard Weinberg, MD, PhD**[a], **James R. Corbett, MD**[a,b,c], **Hakan Oral, MD**[a], **Venkatesh L. Murthy, MD, PhD**[a,c]

[a]Department of Medicine (Division of Cardiovascular Medicine), University of Michigan, Ann Arbor, MI

[b]INVIA Medical Imaging Solutions, Ann Arbor, MI

[c]Division of Nuclear Medicine, Department of Radiology, University of Michigan, Ann Arbor, MI

[d]Department of Medicine (Division of Cardiovascular Medicine), Massachusetts General Hospital, Harvard Medical School, Boston, MA

Abstract

Background.—Left atrial (LA) remodeling is associated with structural, electric, and metabolic LA changes. Integrated evaluation of these features *in vivo* is lacking.

Methods.—Patients undergoing ^{18}F-fluorodeoxyglucose (FDG) PET-CT during a hyperinsulinemic-euglycemic clamp were classified into sinus rhythm (SR), paroxysmal AF (PAF), and persistent AF (PerAF). The LA was semiautomatically segmented, and global FDG uptake was quantified using standardized uptake values (SUVmax and SUVmean) in gated, attenuation-corrected images and normalized to LA blood pool activity. Regression was used to relate FDG data to AF burden and critical patient factors. Continuous variables were compared using t-tests or Mann-Whitney tests.

Results.—117 patients were included (76% men, age 66.4 ± 11.0, ejection fraction (EF) 25[22–35]%) including those with SR (n = 48), PAF (n = 55), and PerAF (n = 14). Patients with any AF had increased SUVmean (2.3[1.5–2.4] vs 2.0[1.5–2.5], P = 0.006), SUVmax (4.4[2.8–6.7] vs 3.2[2.3–4.3], P < 0.001), uptake coefficient of variation (CoV) 0.28[0.22–0.40] vs 0.25[0.2–0.33], P < 0.001), and hypometabolic scar (32%[14%−53%] vs 16.5%[0%−38.5%], P = 0.01). AF burden correlated with increased SUVmean, SUVmax, CoV, and scar independent of age, gender, EF, or LA size (P < 0.03 for all).

Reprint requests: Venkatesh L. Murthy, MD, PhD, Department of Medicine (Division of Cardiovascular Medicine), University of Michigan, 1500 E. Medical Center Dr. SPC 5873, Ann Arbor, MI 48109; vlmurthy@med.umich.edu.

Electronic supplementary material The online version of this article (https://doi.org/10.1007/s12350-018-1429-y) contains supplementary material, which is available to authorized users.

The authors of this article have provided a PowerPoint file, available for download at SpringerLink, which summarises the contents of the paper and is free for re-use at meetings and presentations. Search for the article DOI on SpringerLink.com.

Conclusions.—LA structure and metabolism can be assessed using FDG PET/CT. Greater AF burden correlates with the increased LA metabolism and scar. (J Nucl Cardiol 2018)

Keywords

Metabolic; PET; cardiomyopathy; echo

INTRODUCTION

Left atrial (LA) remodeling is a complex and poorly understood process that occurs in a variety of disease states and is an important driver of atrial fibrillation (AF). Remodeling manifests as electrical, structural, and functional LA changes which are interrelated.[1–3] For example, untreated AF has been postulated to promote LA dilation and fibrosis, which may be reversible with restoration of sinus rhythm (SR).[4] Remodeling is believed to be driven by altered atrial metabolism though both cellular and extracellular pathways.[5,6] Altered metabolism is a known component of ventricular remodeling[7–10] and similar mechanisms are likely involved in atrial tissue as well. Understanding the interplay of atrial metabolism, fibrosis, remodeling and the clinical AF syndrome could have important mechanistic and clinical implications. Parsing out these complex relationships remains challenging, in part due to a limited means for joint quantification of LA remodeling and metabolism in humans.

To date, nearly all imaging studies of the LA have used anatomic imaging methods such as cardiac magnetic resonance imaging (cMRI), computed tomography (CT), and echocardiography to assess volumes, function, and, in emerging data, fibrosis. Nuclear techniques enable quantitative, noninvasive assessments of tissue and organ physiology, though historically this has not been feasible in the LA due to limited spatial resolution. With improving imaging technology using positron emission tomography (PET) imaging and advanced image reconstruction methods, visualization of the LA on ^{18}F-fluorodeoxyglucose (FDG)PET/CT is becoming feasible and has been the subject of case reports and small case series.[11–13] This technique, imaging cellular uptake of a glucose analog, is a gold standard technique for identification of left ventricular scar/fibrosis and can be used to measure left ventricular metabolism and to assess volumetric and functional parameters. Importantly, demonstration of feasibility of PET/CT of the LA could form a basis for application of emerging radiotracers to interrogate many other aspects of AF pathophysiology.

We performed a retrospective, pilot study that sought to understand the feasibility of FDG PET/CT to relate scar and metabolic parameters identified by this method with structural remodeling across patients with varying degrees of AF burden. We hypothesize that patients with AF will have significant perturbations in global and regional atrial metabolisms that are quantifiable and correlative with AF burden.

METHODS

Study Population

Patients referred for FDG PET/CT rest and stress cardiac viability study at the University of Michigan (Ann Arbor, MI) between 01/01/2013 and 04/30/2016 were identified using relevant CPT codes. Patients whose images were missing or uninterpretable owing to poor image quality were excluded. A diagnosis of AF was confirmed by review of 12-lead EKG and classified according to multisociety guidelines; paroxysmal AF was defined as AF that terminates spontaneously or with intervention within 7 days of onset, persistent AF is continuous AF that is sustained for>7 days.[14] The effect of AF burden on imaging parameters was assessed by comparing patients with histories of no AF, paroxysmal AF, and persistent AF. A small number of FDG-uptake images were available from healthy volunteers who had undergone an identical imaging protocol and were analyzed for reference FDG-uptake values. This study was approved by the University of Michigan Institutional Review Board and conducted in accordance with institutional guidelines.

Patient Preparation and Imaging

Patients were instructed to fast overnight for at least 8 hours and to abstain from caffeine and methylxanthines. Patients being treated with short acting insulin or oral hypoglycemic agents were asked to hold their morning doses. Nighttime long-acting insulin doses the prior evening were halved. All patients underwent rest and, where indicated, regadenoson stress perfusion imaging (n = 26) with weight adjusted Rb-82 (13–45mCi), as previously described[15] using a Siemens mCT PET/CT system (Siemens Medical Imaging, Knoxville, TN). In patients undergoing stress testing, the effects of regadenoson were reversed with aminophylline 150mg IV prior to FDG imaging. Following perfusion imaging, patients underwent a hyperinsulinemic-euglycemic clamp protocol, which is clinical routine practice at our institution and which typically occurs 30–60 minutes after stress testing. Briefly, insulin was infused intravenously at 0.2 units/kg/hr. 20% dextrose was infused at a starting rate of 1.5 ml/kg/hr and titrated to achieve a steady state of stable fingerstick glucose between 100 and 140 mg/dl. Patients were then injected with 8–10 mCi of FDG based on body weight followed by PET/CT imaging performed approximately 50 minutes later and at least three hours post stress testing.

Imaging Protocols and Reconstruction

All imaging was performed in the supine position and, wherever possible, with the patient's arms raised above the head. Following a low-dose CT scan for attenuation correction, imaging was performed in list mode for 7 minutes for Rb-82 perfusion imaging and for 15 minutes for FDG imaging. Images were reconstructed using 3-dimensional ordered subsets expectation maximization reconstruction, an advanced iterative image reconstruction method with modeling of system response to maximize resolution recovery, incorporating photon time-of-flight data. Images were reconstructed using an 128×128 matrix size with Gauss 7mm filtering.

After reconstruction, images were analyzed using Corridor 4DM software (INVIA Medical Imaging Solutions, Ann Arbor, MI). All FDG PET/CT studies were reviewed by

experienced observers, who were blinded to the diagnosis of atrial fibrillation. Rest and stress left ventricular (LV) ejection fractions (EFs) and volumes were calculated from gated myocardial perfusion images. Semiquantitative 17-segment visual interpretation of the gated myocardial perfusion images was using a standard 5-point scoring system.[16] Summed rest (SRS) and stress scores (SSS) were calculated as the sum of individual segmental scores on the respective images, and their difference was recorded as summed difference score. For each of these variables, higher scores reflect larger areas of myocardial ischemia and/or scar. Summed rest, stress, and difference scores were converted into percentages of total myocardium by division of the maximum possible score.

LA Segmentation and Assessment

LA FDG uptake was assessed by semiautomatically tracing a region of interest (ROI) along the left atrium using fused PET/CT images (Figure 1). Manual adjustment of contours was required in all cases and required approximately 5 minutes per subject. The entire interatrial septum was considered to be part of the left atrial tissue. ECG gated images were used to adjust for cardiac movement and define valve planes, low-dose CT images were used to confirm our contours and exclude extra-cardiac structures. FDG-uptake counts were summed across all gated images for quantification. Quantitative measurements of FDG uptake were made using standardized uptake values (SUVmax and SUVmean) in the attenuation-corrected images. FDG uptake coefficient of variation (CoV) was also calculated. To correct for blood pool FDG activity, target to background ratios (TBR) were calculated for all patients by normalizing the left atrial SUV for blood pool activity in the LA. In order to compute the proportion of scar within the atria, we compared the normalized atrial FDG uptake in polar map format with a uniform distribution and computed the percentage of atrium below 50% of peak metabolic activity. As with left ventricular defect quantification, Corridor 4DM software utilizes a contiguous region of 10 sampled points to define the peak intensity for normalization of LA-uptake intensity. The cut-off of \50% peak uptake used to define atrial scar is the same used to define nonviable left ventricular tissue.[17] Composite distributions across rhythm categories were constructed by averaging the left atrium FDG-uptake distributions across all patients in the sinus, paroxysmal AF and persistent AF groups.

Echocardiography Imaging

All patients had transthoracic echocardiography (TTE) images available for review. Images were reviewed by a single expert (HY) using commercially available software. LV size was measured in the parasternal long axis view using internal cavity dimensions at peak systole and diastole, LV EF was measured using the biplane method of disks, and LA volume was calculated using the ellipsoid model.[18,19] Mitral regurgitation was defined as none, mild, moderate or severe, per national guideline definitions.[20]

EKG Analysis

Standard 12 lead EKGs were retrospectively reviewed by a single expert (MG). Only patients with sinus P-waves on an EKG within one month of imaging were included, others were excluded due to persistent atrial or ventricular pacing, EKGs only demonstrating atrial fibrillation, or uninterpretable or missing EKGs. P-wave indices were defined using

previously published methods[21]; the PR interval (in milliseconds) was defined by measurement from the onset of the P-wave to the initiation of the QRS segment. The mean value across all 12-leads was used. P-wave duration (in milliseconds) was measured from the P-wave onset (conclusion of the T-P segment) to its offset (return to baseline for the remaining PR interval) and was measured as the mean over all leads. P-wave terminal force (μVms), specific to right precordial lead V1, was determined as the product of the negative P-wave deflection in lead V1 (in μV) and the duration (in milliseconds) from the onset of the negative deflection to its nadir.

Statistical Analysis

All continuous variables were assessed for normality with the Shapiro-Wilk test. Where appropriate, deviations from normality were mitigated by natural log transformation. Continuous variables are presented as medians and intraquartile ranges or means and standard deviations, as appropriate based on normality. Categorical data are summarized as frequencies and percentages. Student's t-test and Mann-Whitney testing were used to compare continuous variables, Chi-square testing was used to compare categorical variables. Pearson and Spearman correlations were used, as appropriate, to quantify correlation between continuous variables. Unadjusted and adjusted regression was performed to assess the influence of clinical parameters (age, gender, ejection fraction, degree of mitral regurgitation (categorized as none/mild, moderate, severe), or LA volume on LA FDG-uptake values. Rhythm status (sinus rhythm, paroxysmal, and persistent atrial fibrillation) was incorporated into regression models as continuous variable as test of trend. ANOVA was used to compare the LA FDG-uptake parameters based on rhythm status. All statistical analyses were performed using R version 3.4.1 (The R Foundation for Statistical Computing, Vienna, Austria).

RESULTS

Study Population and Reference SUV-Uptake Values

We identified 118 patients who had undergone clinically indicated cardiac FDG PET/CT for assessment of myocardial viability. One patient was excluded due to missing imaging data for a final study population of 117, Table 1. The average glucose level prior to tracer injection was 106 ± 9.9 mg/dL with no significant differences between subgroups of AF (P>0.05). The average time from FDG injection to image acquisition was 55.6 ± 12.5 minutes, with no significant differences between subgroups of AF (P>0.05). The LA was successfully contoured and analyzed in all remaining subjects (117/117, 100%). The population was predominantly male (76%, n = 89) with a mean age of 66.4 ± 11.0. 59% had a history of AF including 12% with a history of persistent AF. Mean ejection fraction on FDG PET/CT was 25.0[18.4–22.2], mean SRS was 20.5 ± 7.95. Among patients with atrial fibrillation, 4% (n = 5 patients with paroxysmal AF) had prior left atrial ablation procedures.

A small number of FDG-uptake images were available from healthy volunteers (n = 5 female, n = 1 male, age = 58[51.25–59] years) who had undergone an identical imaging protocol and were analyzed for reference FDG-uptake values.

Maximum and Mean LA Metabolisms

Patients with any AF had higher mean metabolic activity (SUVmean 2.3[1.5–2.4] vs 2.0[1.5–2.5], $P = 0.006$), and peak metabolic activity (SUVmax 4.4[2.8–6.7] vs 3.2[2.3–4.3], $P<0.001$), compared to those without AF, Table 1. Reference values from healthy volunteers were SUVmean of 0.65[0.6–1.1] and SUVmax 1.15[1.0–1.5]. Mean and maximum atrial metabolism values were increased in patients with a higher AF burden (Figure 2A and 2B) ($F = 4.61$, $P<0.02$ and $F = 7.08$, $P<0.001$, respectively). Adjusted regression analysis demonstrated that AF burden was associated with the increased SUVmax and SUV mean values independent of critical covariates ($P<0.01$ for both).

LA Metabolic Heterogeneity

Metabolic activity was more heterogeneous across the LA in patients with any AF than those without (CoV 0.28[0.22–0.40] vs 0.25[0.2–0.33], $P<0.001$). Reference values from healthy volunteers was CoV 0.20[0.14–0.33]. Adjusted regression analysis demonstrated that, rhythm status (sinus rhythm, paroxysmal AF, persistent AF) was associated with an increase in FDG CoV independent of critical covariates ($P = 0.005$).

Composite polar maps of metabolic distribution normalized to peak uptake are displayed in Figure 3. There was greater heterogeneity of LA metabolic activity in patients in persistent AF (LA FDG uptake relative to peak uptake, sinus rhythm 67.0 ± 7.6%, paroxysmal AF 62.3 ± 9.3%, persistent AF 59.3 ± 10.4%).

Hypometabolic LA Scarring

Patients with AF were found to have a greater percentage of hypometabolic scar (32%[14% −53%] vs 16.5%[0%−38.5%], $P = 0.01$), Figure 4. Reference values from healthy volunteers were hypometabolic scar were. 2.5[0.50–8.25]%. Blackout maps were compared in patients with SR, paroxysmal AF, and persistent AF and there was an increase in LA scar related to AF burden ($F = 3.34$, $P = 0.03$), Figure 2C. Adjusted regression analysis demonstrated that increased AF burden was associated with increased LA scar independent of critical covariates ($P = 0.02$).

Patients with increased atrial metabolism were found to have increased areas of hypometabolic scar; SUVmean and SUVmax were moderately correlated with the percentage of hypometabolic LA scar (rho 0.56, $P<0.01$ and rho 0.75, $P<0.01$ respectively) (Figure 5A and 5B).

LA Volume Assessment by PET and Echocardiography

The mean duration between imaging acquisition and TTE studies analyzed was 28 ± 46 days. The mean TTE-derived LA diameter was 4.8 ± 0.7cm and median LA volume was 94.0[73.0–118.0] cm^3. There was strong correlation between LA volume derived by surface echocardiography and PET-derived LA linear measurements (Pearson R = 0.88+/−0.04, $P<0.001$). PET-derived LA volumes were increased in patients with AF (90.6[72.5–103.1] vs 104.9[82.5–131.7], $P = 0.005$). AF burden was associated with larger LA volumes independent of age, gender, or ejection fraction ($P<0.001$).

LA FDG Uptake and Atrial and Ventricular Structures

Atrial metabolism showed weak, to no correlation with measures of LV size, function, and scar, Table 2. LA scar was weakly correlated with LA volumes (rho 0.18, $P = 0.04$) but no other structural parameters. LA volumes were weakly correlated with maximum LA metabolism (rho 0.18, $P = 0.04$) but not mean LA metabolism.

LA FDG Uptake and P-Wave Parameters

EKGs were analyzed in patients with sinus rhythm ($n = 43$) and paroxysmal AF ($n = 28$), the remaining patients had either persistent AF ($n = 14$), no recent EKGs in sinus rhythm ($n = 10$), paced atrial rhythm ($n = 20$), or had EKGs unsuitable for interpretation ($n = 2$). The average time between image acquisition and EKG analyzed was 8 ± 14 days. P-wave terminal force was modestly correlated with both maximum and mean atrial metabolisms ($\rho = 0.27$, $P = 0.02$ and $\rho = 0.29$, $P = 0.01$, respectively). No other correlation between p-wave indices and LA FDG-uptake values were found (Table 3).

DISCUSSION

We performed multiparametric LA measurements simultaneously using a single FDG PET/CT imaging protocol, employing advanced image reconstruction techniques to maximize image resolution. Our results were consistent with existing models of LA remodeling while adding information on atrial metabolism measured *in vivo*. We demonstrate that patients with AF have greater LA volumes, increases in the amount and heterogeneity of LA metabolism, and greater amounts of LA scar. These results demonstrate the feasibility of FDG imaging of the atrial substrate using existing techniques.

Atrial Fibrillation and Metabolism

Patients with higher AF burdens and those with increased p-wave terminal forces (associated with atrial hypertrophy and pressure overload states[22,23]) had increased atrial metabolism.. Rapid and continuous activity of the atria during AF leads to an oxygen imbalance resulting in atrial hyperemia, altered oxygen reactive speciation processing, and abnormal calcium homeostasis among other derangements.[24,25] A transient supply-demand mismatch may progress to a chronic hypoxic state in patients with persistent AF leading to progressive cellular and vascular changes. During periods of hypoxia, ventricular myocytes shift from preferential utilization of fatty acids towards glucose.[26] The energy preferences of atrial myocytes during baseline and stressed states are unknown[27]; however, our findings of increased FDG uptake associated with states of atrial stress may suggest a similar process.

Atrial Fibrillation and Scar Burden

Quantification of atrial scar as a measure of structural remodeling is an emerging tool and has implications for AF treatment and prognosis.[28] Using FDG imaging we found increased areas of hypometabolic scar in patients with AF that were dependent on AF burden (Figure 2C). Similar results have been shown in studies using late gadolinium enhancement (LGE) cMRI to detect LA fibrosis.[29] Unfortunately correlative MRI data were not available in this study though demonstration of spatial coregistration of areas of LGE with areas of hypometabolic scar is an important next step for future prospective studies.

Histologic and imaging data have demonstrated the close relationship between AF burden LA fibrosis.[30,31] LA fibrosis can occur in both homogeneous/dense patterns as well as nonconfluent patterns. Correlation with intracardiac electrograms has shown that these nonconfluent or patchy areas of fibrosis are more likely to harbor areas of atrial substrate supportive of AF than are areas of homogenous/dense fibrosis.[32] This may explain our observation of increased atrial metabolism heterogeneity with more long-standing AF; however, given the spatial resolution limitations of FDG-uptake assessment, we cannot delineate the fibrotic phenotype (dense vs patchy). A recent feasibility study using PET/MRI overlay demonstrated that localization of scar formation post-catheter ablation is possible.[33] Multimodality imaging using PET-derived metabolic information could yield additional insights into LA remodeling.

Atrial Metabolism and Structural Remodeling

Increased atrial volume and scar burden were correlated with increased atrial metabolism. Abnormal metabolism may be early steps in a cascade of changes that result in gross atrial remodeling though evidence for this is largely circumstantial.[27] One proposed mechanism describes chronic energy starvation activating pathways linked to cell death and cardiomyopathy.[34]

Our findings suggest that patients with advanced AF have progressively scarred atria with relative increased metabolism in viable atrial regions. A compensatory increase in energy utilization could be expected to maintain atrial contractility in the setting of progressive dilation, scaring, and atrial stiffness. Animal models have demonstrated that AF induces reactive hyperemia[35] and changes in mitochondrial ATP synthase expression[36] to support increased energy demands. The extent to which atrial myocytes can compensate to these metabolic demands are unknown. Future studies incorporating metabolomic and proteomic profiles may add to the biological plausibility of these findings.

There was no correlation between atrial metabolism or scar and LV functional parameters such as ejection fraction and LV chamber remodeling. Ventricular remodeling and resulting diastolic dysfunction are known to be related to LA function and remodeling.[37] The lack of association likely results from the skewed patient population where most had severe cardiomyopathy. We would expect that a more heterogenous population would better demonstrate these relationships and should be the focus of future studies.

Prior Studies of Atrial FDG Uptake

This is the largest series to characterize LA FDG uptake in patients and the only study to examine the impact of AF burden on these parameters. Lange *et al.* reported a case-control series of 72 patients with sinus rhythm and atrial fibrillation and found only a mild increase in LA FDG uptake that did not meet statistical significance.[38] The protocol in that study used a brief fast for metabolic preparation which may partially suppress myocardial glucose metabolism and thus could not readily differentiate between myocardial scar and normal areas. In addition, that study utilized five discreet regions of interest (ROI) to assess atrial FDG uptake (as opposed to imaging the entire LA) which may have less ability to identify regional heterogeneity compared to volumetric methods. Other smaller case series have

reported similar findings of increased atrial uptake on FDG[39,40] using a single ROI which incorporated the entire atrial chamber, but without detailed exploration of regional heterogeneity.

LA Wall Thickness and FDG Uptake

There exists both intra- and interpatient variability in LA wall thickness.[41] We were unable to account for regional LA thickness in this pilot study and it is unknown to what extent FDG-uptake differences are due to variations in wall thickness vs a difference in the rate of tissue glucose utilization per unit mass of tissue. The relationship between wall thickness and atrial metabolism is likely not directly correlative. For example, in our small sample of control patients we observed relatively homogenous FDG uptake despite likely heterogenous LA wall thickness described in healthy cohorts. High-density electroanatomic mapping studies have demonstrated that increased LA wall thickness can harbor greater areas of scar tissue and presumably lower metabolic activity.[42] Future studies should evaluate the role of regional LA wall thickness and FDG uptake.

Clinical Implications

The evaluation of atrial substrate has important clinical applications. In a large prospective study, the degree of LA fibrosis assessed by LGE cMRI predicted the risk of AF recurrence after catheter ablation and conversion to sinus rhythm.[30] Scar assessment may assist in selection, risk stratification, and procedural approaches in patients undergoing ablation.[43] However, a recent study utilizing imaging protocols available at the majority of imaging centers was unable to detect or quantify atrial scar using LGE-MRI leading the authors to question the real-world application of this technique.[44] Additional patient level factors (implantable cardiac devices, renal dysfunction, claustrophobia, et cetera) may limit the use of LGE-MRI. FDG PET-CT may provide complimentary information to LGE-MRI using available imaging equipment with minimal post-acquisition processing.

LA remodeling is related to the risk of thromboembolism in patients with AF independent of arrhythmia burden alone.[45] Better identification of patients at high risk for complications of AF would allow for tailored treatment strategies. LA remodeling is related to a variety of disease states including hypertension, heart failure with preserved ejection fraction, obstructive sleep apnea, and obesity.[45–48] Prognostic information, response to therapeutics, and new mechanistic insight could be obtained from application of FDG PET-CT imaging in these populations.

Limitations

This is an observational study, which carries the potential for selection bias among other limitations. PET-CT scans were performed in patients undergoing cardiac viability assessments, and accordingly, the population consisted of patients with severe structural heart disease, which limits the generalizability of these results. However, we would expect that a more heterogenous population could increase the observed range of differences across rhythm categories. Clinical outcomes, response to therapies, and evolution of LA remodeling were not assessed due to the nature of the patient population and lack of follow-

up imaging. AF ablation procedures contribute to LA scaring, [49] which may impact FDG uptake and heterogeneity patterns, although we were unable to adjust for this variable. We did not address the effect of rhythm status during imaging or acute hemodynamics (blood pressure, volume status) during FDG imaging. We would expect that increased LV end-diastolic pressure could impact LA metabolism independent of rhythm status. These questions should be examined in larger studies utilizing serial scans in patients with sinus rhythm vs AF, pre and post ablation, and with simultaneous hemodynamic measurements. Our data describe trends in the LA in its entirety although there are anatomically and physiologically distinct structures (left atrial appendage, pulmonary vein ostium, posterior wall, et cetera) which will be described in future studies.

Future studies should incorporate FDG PET-CT and cardiac MRI findings. This will allow for validation of atrial scar measurement, assessment of regional variations in FDG uptake, assess the impact of regional atrial wall thickness on FDG uptake, and incorporate functional parameters such as LA EF into our model.

Finally, we employed state-of-the-art reconstruction techniques to improve image resolution to allow quantification of the left atrium. Yet imaging of the left atrium is challenging, and partial volume effects may impair quantification. However, this should bias results towards the null. Future multimodality efforts could more accurately incorporate models for atrial wall thickness and partial volume effects.

CONCLUSION

In this pilot study, we demonstrate that multiparametric assessment of the LA can be performed with FDG PET/CT imaging using advanced image reconstruction protocols. The use of this modality as a novel tool to study electric, structural, and metabolic aspects of the LA should be further explored (Figure 6).

Supplementary Material

Refer to Web version on PubMed Central for supplementary material.

NEW KNOWLEDGE GAINED

This study demonstrates the feasibility of FDG PET/CT as a new modality to study LA remodeling *in vivo*. We report the largest and most complete evaluation of LA metabolism assessed via FDG uptake and show new relationships between electric, structural, and metabolic remodeling.

Disclosure

Drs. Ficaro and Corbett own equity in INVIA Medical Imaging Solutions. Dr. Murthy owns stock in General Electric and Cardinal Health, owns stock options and has received consulting fees from Ionetix, and has received research grants from Siemens Medical Imaging. Dr. Murthy is supported by Grant R01HL136685 from the National, Heart, Lung, and Blood Institute and R01AG059729 from the National Institute on Aging. Drs. Ghannam, Yun, Ghanbari, Lazarus, Konerman, Shah, Weinberg, and Oral have no disclosures or conflicts of interest related to this publication.

Abbreviations

LA	Left atrium

AF	Atrial fibrillation
cMRI	Cardiac magnetic resonance imaging
CT	Computed tomography
FDG PET/	^{18}F-fluorodeoxyglucose positron
CT	emission tomography/computed tomography
SUV	Standardized uptake values
CoV	Coefficient of variation
EF	Ejection fraction
LGE	Late gadolinium enhancement

References

1. Morillo CA, Klein GJ, Jones DL, Guiraudon CM. Chronic rapid atrial pacing. Structural, functional, and electrophysiological characteristics of a new model of sustained atrial fibrillation. Circulation 1995;91:1588–95. [PubMed: 7867201]
2. Wijffels MC, Kirchhof CJ, Dorland R, Allessie MA. Atrial fibrillation begets atrial fibrillation. A study in awake chronically instrumented goats. Circulation 1995;92:1954–68. [PubMed: 7671380]
3. Mahajan R, Lau DH, Brooks AG, Shipp NJ, Manavis J, Wood JP, Finnie JW, Samuel CS, Royce SG, Twomey DJ, Thanigaimani S, Kalman JM, Sanders P. Electrophysiological, electroanatomical, and structural remodeling of the atria as consequences of sustained obesity. J Am Coll Cardiol 2015;66:1–11. [PubMed: 26139051]
4. Walters TE, Nisbet A, Morris GM, Tan G, Mearns M, Teo E, Lewis N, Ng A, Gould P, Lee G, Joseph S, Morton JB, Zentner D, Sanders P, Kistler PM, Kalman JM. Progression of atrial remodeling in patients with high-burden atrial fibrillation: Implications for early ablative intervention. Heart Rhythm 2016;13:331–9. [PubMed: 26484789]
5. Souders CA, Bowers SL, Baudino TA. Cardiac fibroblast: the renaissance cell. Circ Res 2009;105:1164–76. [PubMed: 19959782]
6. Dzeshka MS, Lip GY, Snezhitskiy V, Shantsila E. Cardiac fibrosis in patients with atrial fibrillation: mechanisms and clinical implications. J Am Coll Cardiol 2015;66:943–59. [PubMed: 26293766]
7. Diamant M, Lamb HJ, Groeneveld Y, Endert EL, Smit JW, Bax JJ, Romijn JA, de Roos A, Radder JK. Diastolic dysfunction is associated with altered myocardial metabolism in asymptomatic normotensive patients with well-controlled type 2 diabetes mellitus. J Am Coll Cardiol 2003;42:328–35. [PubMed: 12875772]
8. Rijzewijk LJ, van der Meer RW, Lamb HJ, de Jong HW, Lubberink M, Romijn JA, Bax JJ, de Roos A, Twisk JW, Heine RJ, Lammertsma AA, Smit JW, Diamant M. Altered myocardial substrate metabolism and decreased diastolic function in nonischemic human diabetic cardiomyopathy: studies with cardiac positron emission tomography and magnetic resonance imaging. J Am Coll Cardiol 2009;54:1524–32. [PubMed: 19815124]
9. Maslov MY, Chacko VP, Stuber M, Moens AL, Kass DA, Champion HC, Weiss RG. Altered high-energy phosphate metabolism predicts contractile dysfunction and subsequent ventricular remodeling in pressure-overload hypertrophy mice. Am J Physiol Heart Circ Physiol 2007;292:H387–91. [PubMed: 16963614]
10. Kundu BK, Zhong M, Sen S, Davogustto G, Keller SR, Taegtmeyer H. Remodeling of glucose metabolism precedes pressure overload-induced left ventricular hypertrophy: review of a hypothesis. Cardiology 2015;130:211–20. [PubMed: 25791172]
11. Dong A, Zhao T, Gong J, Zuo C. Diffuse FDG uptake of the bilateral atrial walls in a patient with atrial fibrillation. Clin Nucl Med 2014;39:167–9. [PubMed: 24217538]

12. Fujii H, Ide M, Yasuda S, Takahashi W, Shohtsu A, Kubo A. Increased FDG uptake in the wall of the right atrium in people who participated in a cancer screening program with whole-body PET. Ann Nucl Med 1999;13:55–9. [PubMed: 10202949]

13. James OG, Christensen JD, Wong TZ, Borges-Neto S, Koweek LM. Utility of FDG PET/CT in inflammatory cardiovascular disease. Radiographics 2011;31:1271–86. [PubMed: 21918044]

14. January CT, Wann LS, Alpert JS, Calkins H, Cleveland JC Jr, Cigarroa JE, Conti JB, Ellinor PT, Ezekowitz MD, Field ME, Murray KT, Sacco RL, Stevenson WG, Tchou PJ, Tracy CM, Yancy CW. 2014 AHA/ACC/HRS guideline for the management of patients with atrial fibrillation: A report of the American College of Cardiology/American Heart Association task force on practice guidelines and the heart rhythm society. J Am Coll Cardiol 2014;64:e1–76. [PubMed: 24685669]

15. Rijnierse MT, de Haan S, Harms HJ, Robbers LF, Wu L, Danad I, Beek AM, Heymans MW, van Rossum AC, Lammertsma AA, Allaart CP, Knaapen P. Impaired hyperemic myocardial blood flow is associated with inducibility of ventricular arrhythmia in ischemic cardiomyopathy. Circ Cardiovasc Imaging 2014;7:20–30. [PubMed: 24343851]

16. El Fakhri G, Kardan A, Sitek A, Dorbala S, Abi-Hatem N, Lahoud Y, Fischman A, Coughlan M, Yasuda T, Di Carli MF. Reproducibility and accuracy of quantitative myocardial blood flow assessment with (82)Rb PET: comparison with (13)N-ammonia PET. J Nucl Med 2009;50:1062–71. [PubMed: 19525467]

17. Dwivedi G, Al-Shehri H, deKemp RA, Ali I, Alghamdi AA, Klein R, Scullion A, Ruddy TD, Beanlands RS, Chow BJ. Scar imaging using multislice computed tomography versus metabolic imaging by F-18 FDG positron emission tomography: A pilot study. Int J Cardiol 2013;168:739–45. [PubMed: 23102604]

18. Pritchett AM, Jacobsen SJ, Mahoney DW, Rodeheffer RJ, Bailey KR, Redfield MM. Left atrial volume as an index of left atrial size: a population-based study. J Am Coll Cardiol 2003;41:1036–43. [PubMed: 12651054]

19. Lang RM, Badano LP, Mor-Avi V, Afilalo J, Armstrong A, Ernande L, Flachskampf FA, Foster E, Goldstein SA, Kuznetsova T, Lancellotti P, Muraru D, Picard MH, Rietzschel ER, Rudski L, Spencer KT, Tsang W, Voigt JU. Recommendations for cardiac chamber quantification by echocardiography in adults: an update from the American Society of Echocardiography and the European Association of Cardiovascular Imaging. Eur Heart J Cardiovasc Imaging 2015;16:233–70. [PubMed: 25712077]

20. Zoghbi WA, Enriquez-Sarano M, Foster E, Grayburn PA, Kraft CD, Levine RA, Nihoyannopoulos P, Otto CM, Quinones MA, Rakowski H, Stewart WJ, Waggoner A, Weissman NJ and American Society of E. Recommendations for evaluation of the severity of native valvular regurgitation with two-dimensional and Doppler echocardiography. J Am Soc Echocardiogr 2003;16:777–802. [PubMed: 12835667]

21. Magnani JW, Zhu L, Lopez F, Pencina MJ, Agarwal SK, Soliman EZ, Benjamin EJ, Alonso A. P-wave indices and atrial fibrillation: cross-cohort assessments from the Framingham Heart Study (FHS) and Atherosclerosis Risk in Communities (ARIC) study. Am Heart J 2015;169(53–61):e1.

22. Tanoue MT, Kjeldsen SE, Devereux RB, Okin PM. Relationship between abnormal P-wave terminal force in lead V1 and left ventricular diastolic dysfunction in hypertensive patients: the LIFE study. Blood Press 2017;26:94–101. [PubMed: 27601135]

23. Goda T, Sugiyama Y, Ohara N, Ikegami T, Watanabe K, Kobayashi J, Takahashi D. P-wave terminal force in lead V1 predicts paroxysmal atrial fibrillation in acute ischemic stroke. J Stroke Cerebrovasc Dis 2017;26:1912–5. [PubMed: 28716584]

24. Simon JN, Duglan D, Casadei B, Carnicer R. Nitric oxide synthase regulation of cardiac excitation-contraction coupling in health and disease. J Mol Cell Cardiol 2014;73:80–91. [PubMed: 24631761]

25. Heijman J, Voigt N, Nattel S, Dobrev D. Cellular and molecular electrophysiology of atrial fibrillation initiation, maintenance, and progression. Circ Res 2014;114:1483–99. [PubMed: 24763466]

26. Liedtke AJ. Alterations of carbohydrate and lipid metabolism in the acutely ischemic heart. Prog Cardiovasc Dis 1981;23:321–36. [PubMed: 7012926]

27. Opacic D, van Bragt KA, Nasrallah HM, Schotten U, Verheule S. Atrial metabolism and tissue perfusion as determinants of electrical and structural remodelling in atrial fibrillation. Cardiovasc Res 2016;109:527–41. [PubMed: 26786160]

28. Han FT, Marrouche N. An atrial fibrosis-based approach for atrial fibrillation ablation. Future Cardiol 2015;11:673–81. [PubMed: 26609731]

29. Khurram IM, Habibi M, Gucuk Ipek E, Chrispin J, Yang E, Fukumoto K, Dewire J, Spragg DD, Marine JE, Berger RD, Ashikaga H, Rickard J, Zhang Y, Zipunnikov V, Zimmerman SL, Calkins H, Nazarian S. Left atrial LGE and arrhythmia recurrence following pulmonary vein isolation for paroxysmal and persistent AF. JACC Cardiovasc Imaging 2016;9:142–8. [PubMed: 26777218]

30. Marrouche NF, Wilber D, Hindricks G, Jais P, Akoum N, Marchlinski F, Kholmovski E, Burgon N, Hu N, Mont L, Deneke T, Duytschaever M, Neumann T, Mansour M, Mahnkopf C, Herweg B, Daoud E, Wissner E, Bansmann P, Brachmann J. Association of atrial tissue fibrosis identified by delayed enhancement MRI and atrial fibrillation catheter ablation: the DECAAF study. Jama 2014;311:498–506. [PubMed: 24496537]

31. Smith JG, Newton-Cheh C, Almgren P, Struck J, Morgenthaler NG, Bergmann A, Platonov PG, Hedblad B, Engstrom G, Wang TJ, Melander O. Assessment of conventional cardiovascular risk factors and multiple biomarkers for the prediction of incident heart failure and atrial fibrillation. J Am Coll Cardiol 2010;56:1712–9. [PubMed: 21070922]

32. Jadidi AS, Cochet H, Shah AJ, Kim SJ, Duncan E, Miyazaki S, Sermesant M, Lehrmann H, Lederlin M, Linton N, Forclaz A, Nault I, Rivard L, Wright M, Liu X, Scherr D, Wilton SB, Roten L, Pascale P, Derval N, Sacher F, Knecht S, Keyl C, Hocini M, Montaudon M, Laurent F, Haissaguerre M, Jais P. Inverse relationship between fractionated electrograms and atrial fibrosis in persistent atrial fibrillation: combined magnetic resonance imaging and high-density mapping. J Am Coll Cardiol 2013;62:802–12. [PubMed: 23727084]

33. Chen S, Kiuchi MG, Acou WJ, Derndorfer M, Wang J, Li R, Kollias G, Martinek M, Kiuchi T, Purerfellner H, Liu S. Feasibility of catheter ablation renal denervation in “mild” resistant hypertension. J Clin Hypertens 2017;19:361–8.

34. Nickel A, Loffler J, Maack C. Myocardial energetics in heartfailure. Basic Res Cardiol 2013;108:358. [PubMed: 23740216]

35. McHale PA, Greenfield JC Jr. Origin of atrial coving in caninephasic coronary artery blood flow. Am J Physiol 1986;251:H774–8. [PubMed: 3766754]

36. Barbey O, Pierre S, Duran MJ, Sennoune S, Levy S, Maixent JM. Specific up-regulation of mitochondrial F0F1-ATPase activity after short episodes of atrial fibrillation in sheep. J Cardiovasc Electrophysiol 2000;11:432–8. [PubMed: 10809497]

37. Lee JS, Shim CY, Wi J, Joung B, Ha JW, Lee MH, Pak HN. Left ventricular diastolic function is closely associated with mechanical function of the left atrium in patients with paroxysmal atrial fibrillation. Circ J 2013;77:697–704. [PubMed: 23196755]

38. Lange PS, Avramovic N, Frommeyer G, Wasmer K, Pott C, Eckardt L, Wenning C. Routine 18F-FDG PET/CT does not detect inflammation in the left atrium in patients with atrial fibrillation. Int J Cardiovasc Imaging 2017;33:1271–6. [PubMed: 28229312]

39. Santi B, et al. Atrial fibrillation is associated with increased atrial metabolic activity on FDG/PET imaging in patients with ischemic cardiomyopathy [Abstract]. Circulation 2015;132. [PubMed: 26100109]

40. Okura K, et al. The characteristics of patients with atrial fibrillation in which 18F-fluorodeoxyglucose accumulate in the atrial wall [Abstract]. JACC 2015;65:A12836.

41. Whitaker J, Rajani R, Chubb H, Gabrawi M, Varela M, Wright M, Niederer S, O’Neill MD. The role of myocardial wall thickness in atrial arrhythmogenesis. Europace 2016;18:1758–72. [PubMed: 27247007]

42. Takahashi K, Okumura Y, Watanabe I, Nagashima K, Sonoda K, Sasaki N, Kogawa R, Iso K, Ohkubo K, Nakai T, Hirayama A. Relation between left atrial wall thickness in patients with atrial fibrillation and intracardiac electrogram characteristics and ATP-provoked dormant pulmonary vein conduction. J Cardiovasc Electrophysiol 2015;26:597–605. [PubMed: 25777254]

43. Akoum N, Daccarett M, McGann C, Segerson N, Vergara G, Kuppahally S, Badger T, Burgon N, Haslam T, Kholmovski E, Macleod R, Marrouche N. Atrial fibrosis helps select the appropriate

patient and strategy in catheter ablation of atrial fibrillation: A DE-MRI guided approach. J Cardiovasc Electrophysiol 2011;22:16–22. [PubMed: 20807271]

44. Bois JP, Glockner J, Young PM, Foley TA, Sheldon S, Newman DB, Lin G, Packer DL, Brady PA. Low incidence of left atrial delayed enhancement with MRI in patients with AF: a singlecentre experience. Open Heart 2017;4:e000546. [PubMed: 28123766]
45. Bisbal F, Gomez-Pulido F, Cabanas-Grandio P, Akoum N, Calvo M, Andreu D, Prat-Gonzalez S, Perea RJ, Villuendas R, Berruezo A, Sitges M, Bayes-Genis A, Brugada J, Marrouche NF, Mont L. Left atrial geometry improves risk prediction of thromboembolic events in patients with atrial fibrillation. J Cardiovasc Electrophysiol 2016;27:804–10. [PubMed: 27027899]
46. Kamioka M, Hijioka N, Matsumoto Y, Nodera M, Kaneshiro T, Suzuki H and Takeishi Y. Uncontrolled blood pressure affects atrial remodeling and adverse clinical outcome in paroxysmal atrial fibrillation. Pacing Clin Electrophysiol 2018.
47. Hohendanner F, Bode D, Primessnig U, Guthof T, Doerr R, Jeuthe S, Reimers S, Zhang K, Bach D, Wakula P, Pieske BM, Heinzel FR. Cellular mechanisms of metabolic syndrome-related atrial decompensation in a rat model of HFpEF. J Mol Cell Cardiol 2017;115:10–9. [PubMed: 29289652]
48. Anter E, Di Biase L, Contreras-Valdes FM, Gianni C, Mohanty S,Tschabrunn CM, Viles-Gonzalez JF, Leshem E, Buxton AE, Kulbak G, Halaby RN, Zimetbaum PJ, Waks JW, Thomas RJ, Natale A, Josephson ME. Atrial substrate and triggers of paroxysmal atrial fibrillation in patients with obstructive sleep apnea. Circ Arrhythm Electrophysiol 2017;10:e005407. [PubMed: 29133380]
49. Peters DC, Wylie JV, Hauser TH, Kissinger KV, Botnar RM, Essebag V, Josephson ME, Manning WJ. Detection of pulmonary vein and left atrial scar after catheter ablation with three-dimensional navigator-gated delayed enhancement MR imaging: Initial experience. Radiology 2007;243:690–5. [PubMed: 17517928]

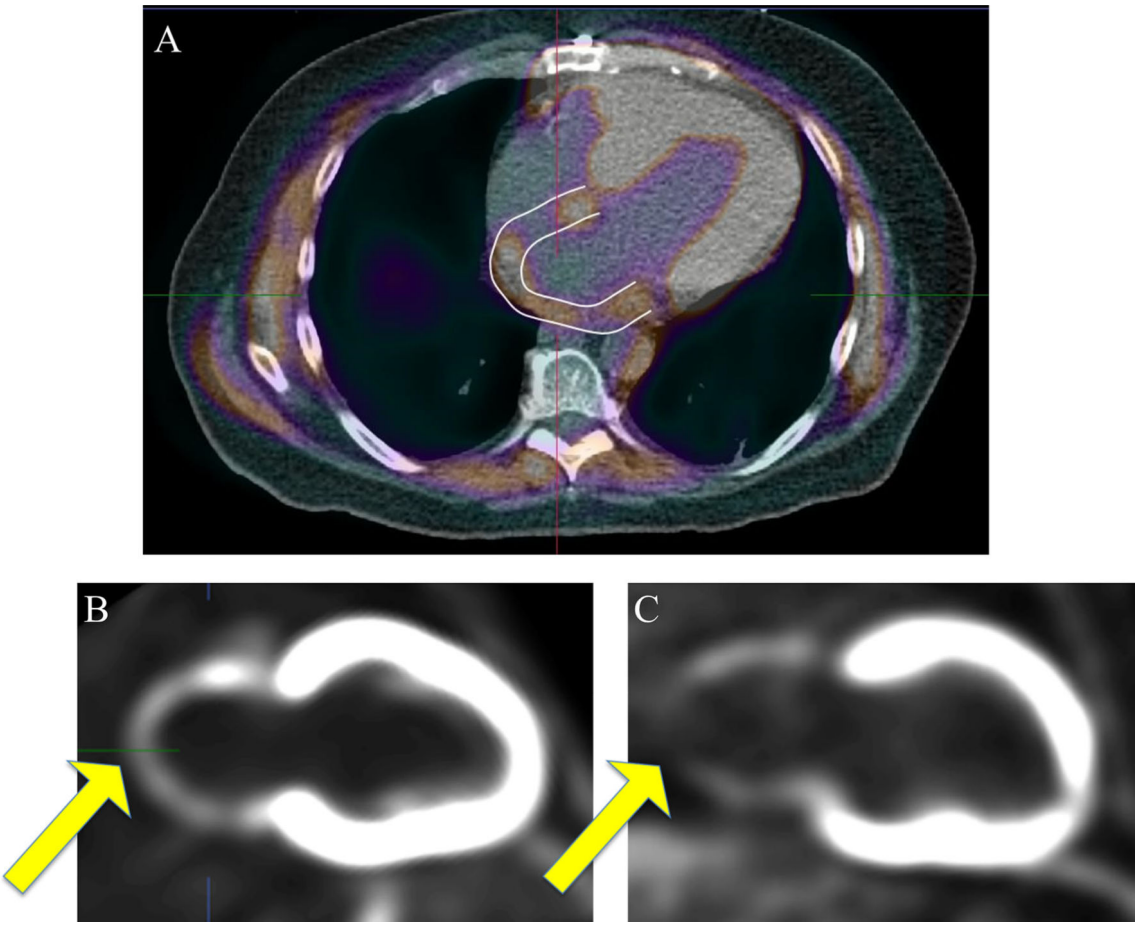

Figure 1.

FDG PET/CT and left atrial area of interest. Integrated FDG and CT imaging with contoured region of interests excluding ventricular and extra-cardiac structure are shown in panel **A.** Vertical long-axis reconstructions showing nonnormalized left atrial FDG-uptake patterns are displayed in panels **B** and **C.** Panel **B** demonstrates relatively homogenous uptake of FDG throughout the atria compared to panel **C,** which demonstrates a defect consistent with hypometabolic scar. CT computed tomography. FDG, ^{18}F-fluorodeoxyglucose.

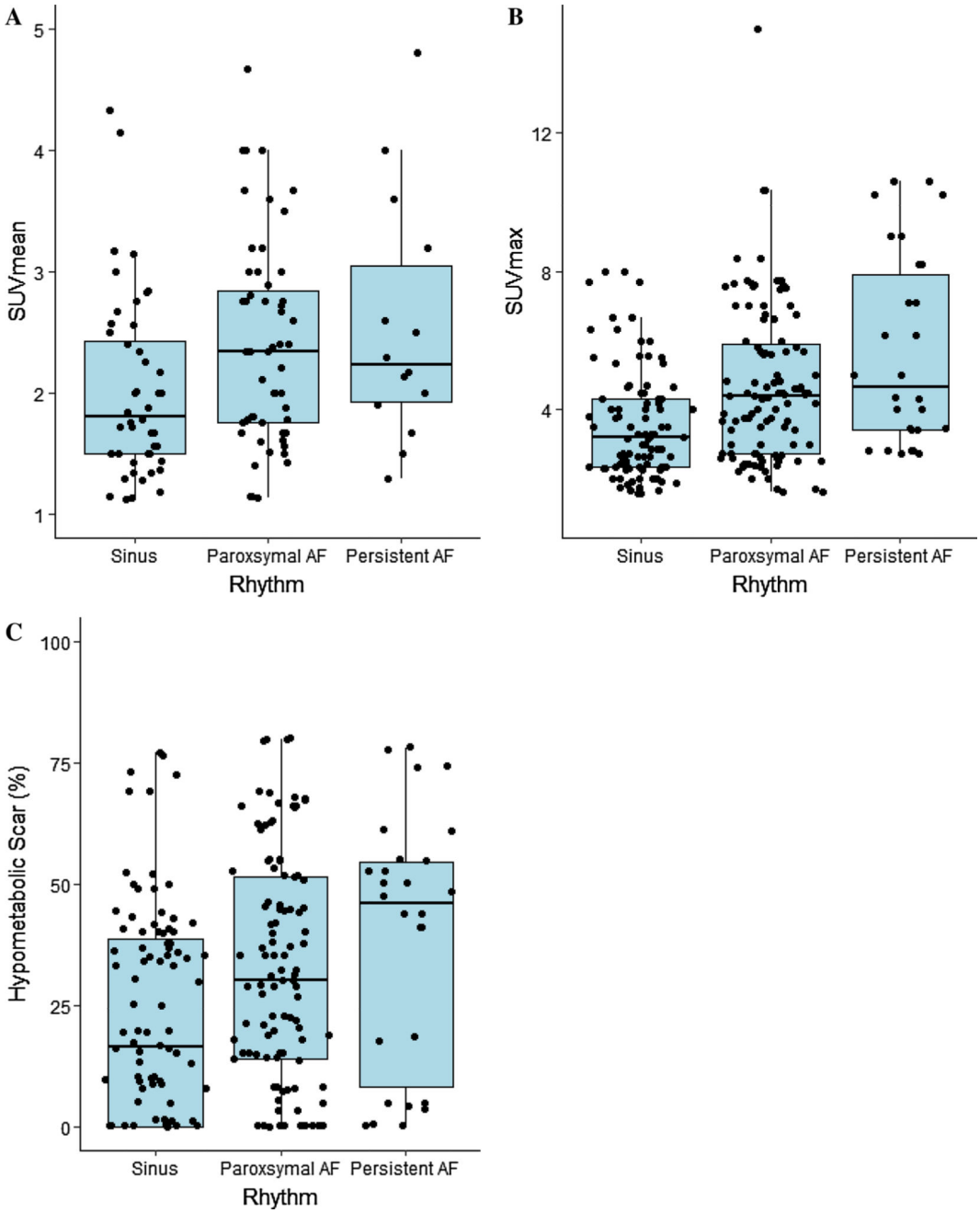

Figure 2.

Left atrial FDG-uptake parameters stratified by rhythm status. **A** SUV mean. **B** SUV max C Blackout 50%, percentage of atrial myocardial tissue uptake below 50% of peak metabolic activity. AF, atrial fibrillation; SUV, standard uptake value; FDG, ^{18}F-fluorodeoxyglucose.

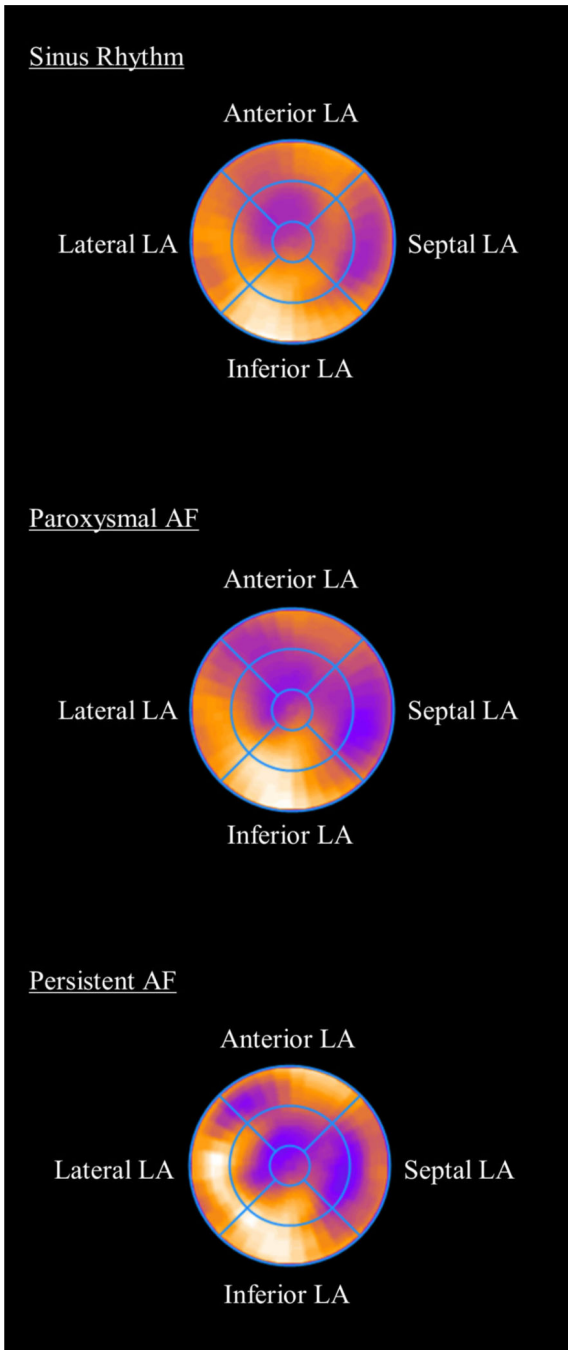

Figure 3.

Polar Maps of Left Atrial Metabolic Uptake. For each patient, LA FDG-uptake distributions were transformed into polar map format and normalized to the peak uptake in the left atrium. Composite distributions were constructed by averaging the left atrium FDG uptake across all patients in the Sinus, paroxysmal AF, and persistent AF groups. Metabolic heterogeneity was increased in patients with a high burden of AF. LA, left atrium; AF, atrial fibrillation.

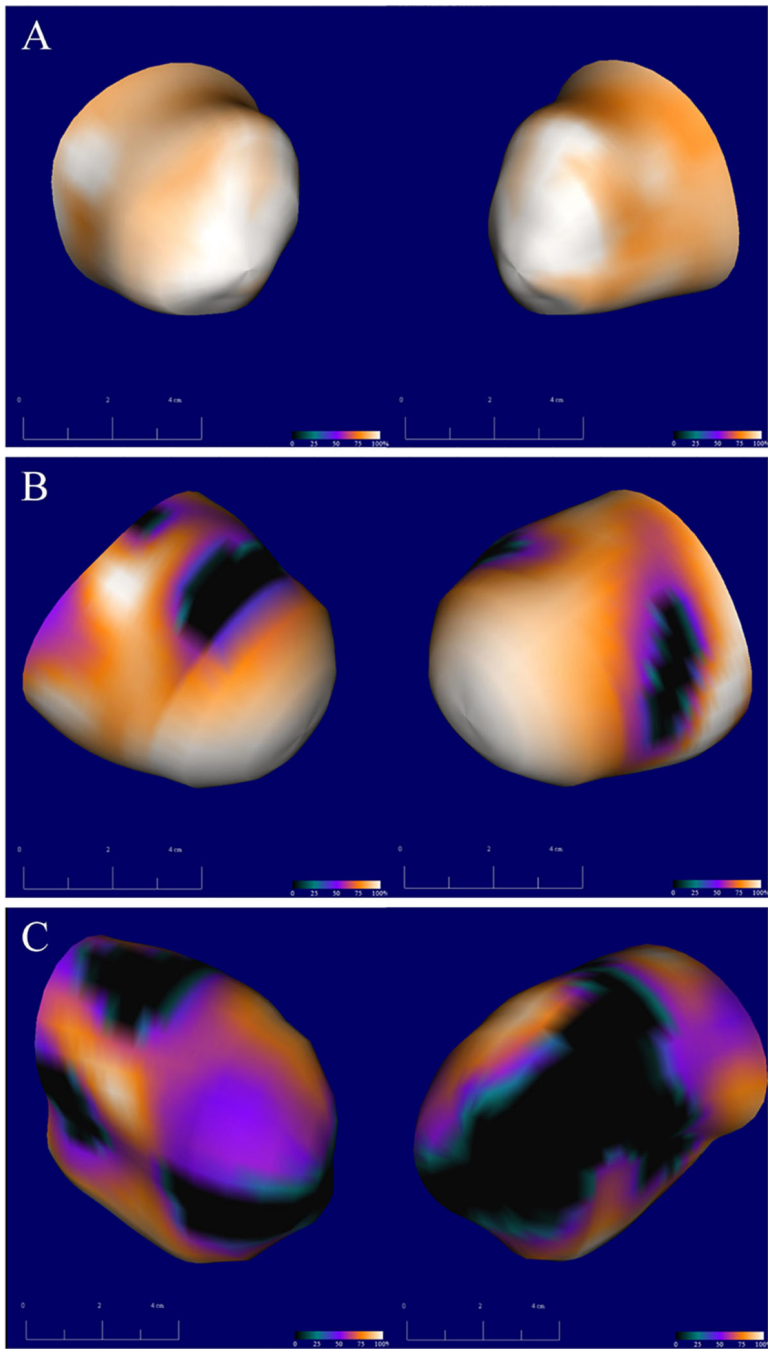

Figure 4.

Left atrial hypometabolic scar: three-dimensional blackout map reconstructions of left atrial metabolic uptake compared to a database of normalized FDG-uptake values. Darker regions represent a greater relative defect in metabolic activity; black regions represent atrial myocardium with less than 50% normalized uptake of FDG consistent with hypometabolic scar. Left posterior oblique and right posterior oblique projections are shown in orthogonal views. Panels **A, B,** and **C** represent three different patients with the increasing amounts of

left atrial scar taken from representative patients with no history of AF (**A**), paroxysmal AF (**B**), and persistent AF (**C**). AF: atrial fibrillation; FDG ^{18}F-fluorodeoxyglucose.

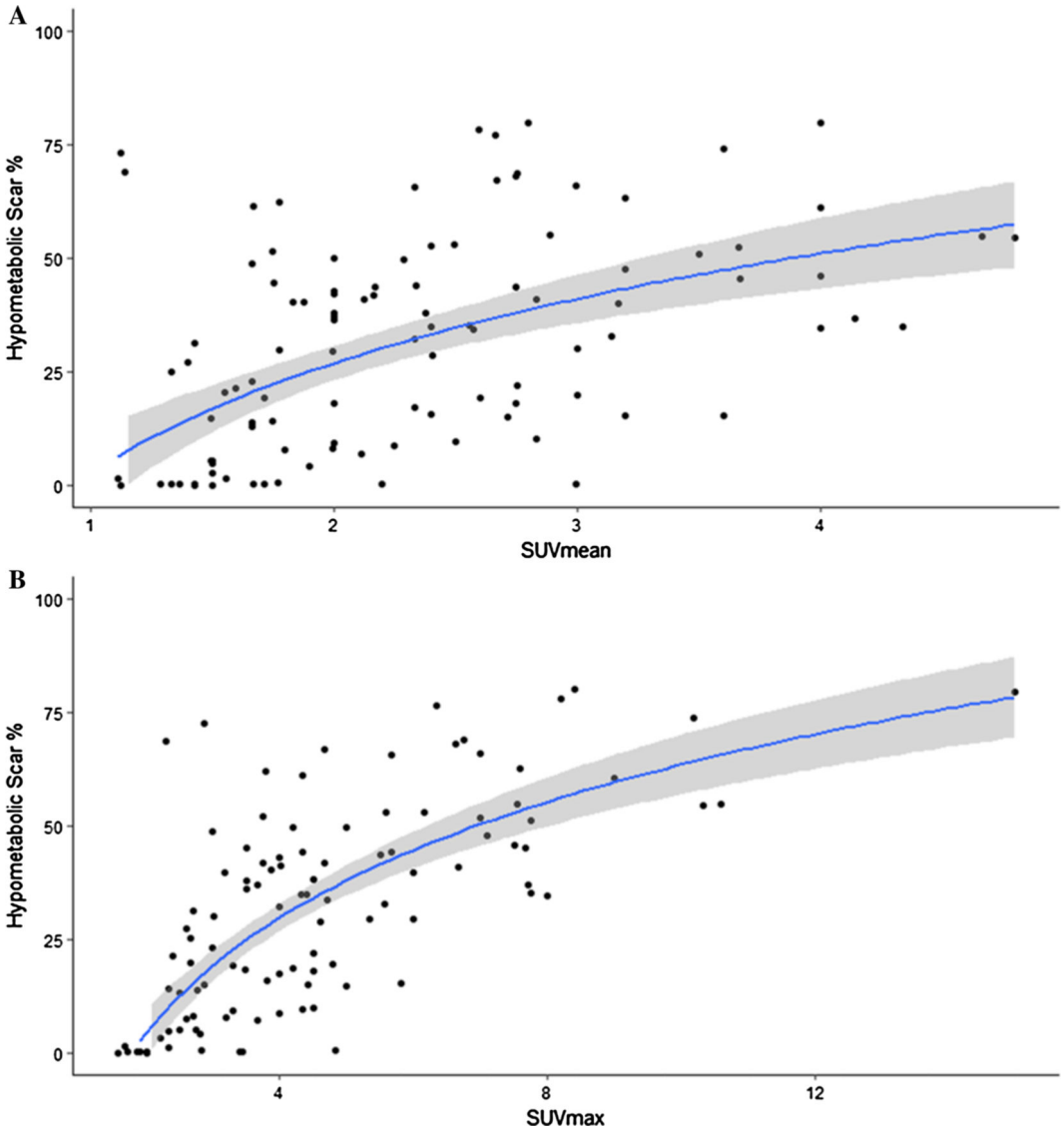

Figure 5.

Hypometabolic scar versus SUVmean and SUVmax. Regression lines and 95% confidence regions are shown. Percentage of atrial myocardial tissue uptake below 50% of peak metabolic activity was compared against **A** mean SUV and **B** max SUV uptakes. SUV, standard uptake value.

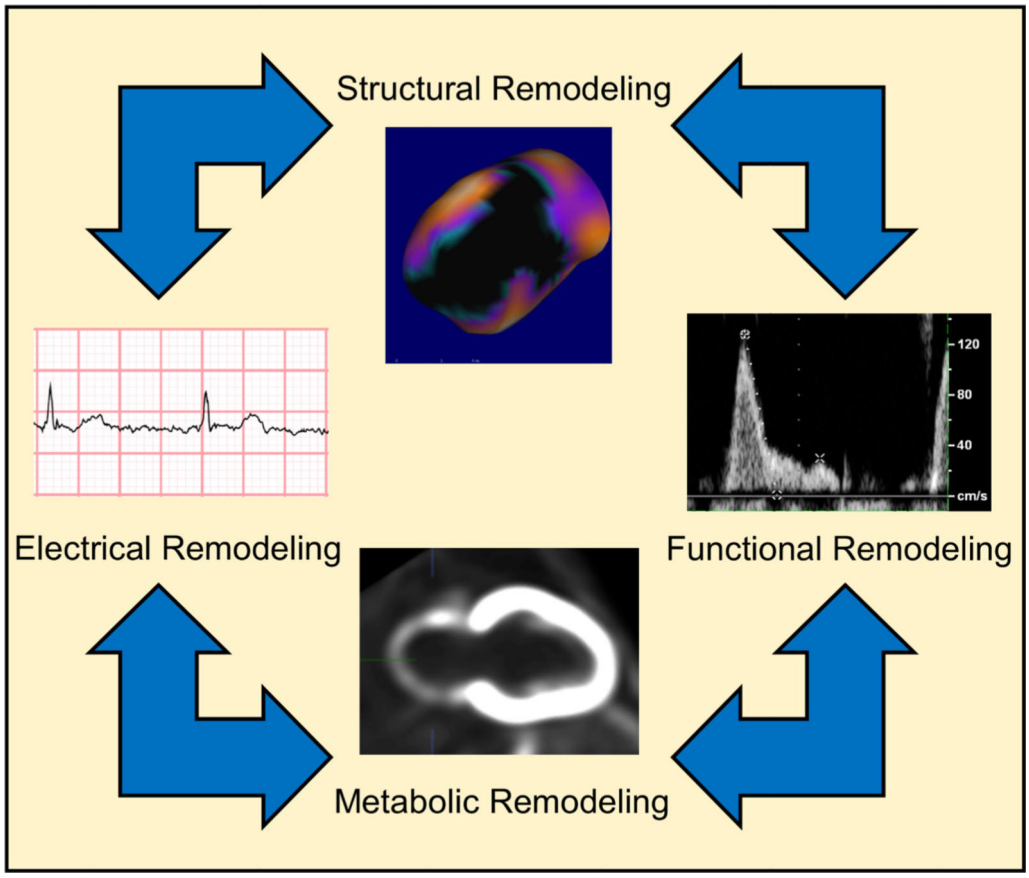

Figure 6.
Left atrial remodeling: left atrial remodeling is the result of the interplay of disturbances of myocardial structure, contractile function, electric properties, and metabolism.

Table 1.

Patient characteristics. Demographic and study data are shown for the total population and stratified by rhythm history

	All (*n* = 117)	Sinus (*n* = 48)	Any AF (*n* = 69)	Paroxsymal AF (*n* = 55)	Persistent AF (*n* = 14)	*P* value
Demographic						
Age	65.5 ± 11.1	62.6 ± 11.6	67.51 ± 10.4	66.45 ± 10.1	71.8 ± 10.5	0.02
Sex (m)	89	33	56	43	13	0.1
BSA	2.0 ± 0.3	2.0 ± 0.3	2.0 ± 0.3	2.0 ± 0.2	2.0 ± 0.2	0.48
Sinus rhythm	41%(48)	na	na	na	na	na
Paroxysmal AF	47%(55)	na	na	na	na	na
Persistent AF	12%(14)	na	na	na	na	na
PET parameters						
Rest EF	25.0[18.4–32.2]	27.5[23.3–32.0]	24.0[20.0–35.5]	24.0[18.5–35.0]	27.0[23.0–35.0]	0.24
EDVI rest	117.0[89.5–143.0]	113.7 ± 39.8	122.7 ± 50.2	126.2 ± 53.2	109.07 ± 34.3	0.32
ESVI rest	82.0[58.0–109.0]	76.5[57.2–108.3]	87.0[63.0–109.0]	88.0[63.0–119.5]	78[60.5–101.5]	0.35
SRS	20.5 ± 8.0	21.8 ± 8.3	19.0 ± 7.6	19.8 ± 7.4	16.0 ± 7.5	0.07
SSS	23.5 ± 9.8	22.2 ± 10.3	23.9 ± 9.9	27.0 ± 7.9	11.5 ± 7.5	0.71
FDG LA volume	95.8[75.7–118.4]	90.6[72.5–103.7]	104.9[82.4–132.7]	99.8[80.9–117.7]	126.5[98.5–161.5]	0.01
FDG LA mean	2.0[1.6–2.7]	1.8[1.5–2.5]	2.3[1.8–2.9]	2.3[1.7–2.8]	2.2[1.9–3.0]	<0.01
FDG LA max	3.8[2.7–5.6]	3.2[2.3–4.3]	4.4[2.8–6.7]	4.4[2.7–5.9]	4.63[3.4–7.9]	<0.01
FDG LA CoV	0.27[.22–.37]	0.25[0.20–0.33]	0.28[0.22–0.40]	0.28[0.24–0.39]	0.32[0.22–0.40]	<0.01
Echo parameters						
Rest EF	25[22–33]	25[20–35]	27[20–36]	25.0[20.0–32.5]	35.0[20.0–36.4]	0.4
LVd diameter	56.6[54.0–66.0]	58.0[52.3–63.8]	60.0[56.0–67.5]	60.0[56.0–67.5]	59.0[55.8–67]	0.17
LVs diameter	50.2[44–56.5]	48.7[41.0–49.0]	50.0[45.0–56.0]	50[45.0–56.0]	48.5[43.3–58.0]	0.85
LA diameter	4.9 ± 0.8	4.5 ± 0.7	5.0 ± 0.8	4.9 ± 0.8	5.2 ± 09	<0.01
LA volume	100.7 ± 39.1	92.2 ± 38.1	106.93 ± 38.87	101.7 ± 37.4	131.7 ± 37.8	0.06
No MR	26%(30)	38%(18)	17%(12)	18%(10)	4%(2)	0.89
Mild MR	47%(55)	38%(18)	54%(37)	53%(29)	57%(8)	<0.01
Moderate MR	20%(23)	21%(10)	19%(13)	20%(11)	14%(2)	0.09
Severe MR	6%(7)	2%(1)	8%(6)	7%(4)	14%(2)	0.01
EKG parameters						

	All (*n* = 117)	Sinus (*n* = 48)	Any AF (*n* = 69)	Paroxsymal AF (*n* = 55)	Persistent AF (*n* = 14)	*P* value
P axis (degree)	47.0[33.5–61.5]	43.0[33.5–58.0]	52.5[34.0–63.0]	51.0[38.5–64.0]	− 35.0[− .35.0 to 35.0]	0.33
PR interval (ms)	170[156–196]	173[154–202]	168[159–192]	176[156–202]	142[142–142]	0.75
P wave duration (ms)	110.9 ± 19.28	107.0 ± 16.1	116.8 ± 22.4	117.3 ± 22.6	104 ± 0	0.04
P wave deflection Max (mv)	112[78–146]	115[78–141]	107[78–156]	112[87–154]	− 112[− 112 to 112]	0.92
P wave terminal force (μVms)	4200[3005–6378]	4182[3143–5635]	4242[2634–7988]	4226[2695–6667]	8364[8364–8364]	0.5

P values represent comparisons between patients with sinus rhythm and a history of atrial fibrillation BSA, Body surface area; AF, atrial fibrillation; EF, ejection fraction; EDVI, end diastolic volume index; EDVS, end systolic volume index; SRS, summed rest score; SSS, summed stress score; FDG, 18F-fluorodeoxyglucose; LA, left atrium; EKG, electrocardiogram; CoV, coefficient of variation; MR, mitral regurgitation; LVd, left ventricular diastolic; LVs, left ventricular systolic; AF, atrial fibrillation; PET, positron emission tomography; ms, miliseconds; lV, microvolts

Table 2.

Correlation of structural parameters to metabolic activity. Spearman rho correlation coefficients between imaging and FDG-uptake parameters

	SUVmean	SUVmax	Blackout 50%
LA volume (cm3)	0.10, P = 0.24	0.18, P = 0.04	0.18, P = 0.04
EF (rest)	− 0.19, P = 0.04	− 0.16, P = 0.07	− 0.09, P = 0.28
EF (stress)	− 0.30, P = 0.11	− 0.28, P = 0.14	−0.25, P = 0.18
EDVI (rest)	0.24, P = 0.007	0.24, P\0.01	0.12, P = 0.21
EDVI (stress)	0.25, P = 0.178	0.212, P = 0.27	0.15, P = 0.45
ESVI (rest)	0.25, P = 0.007	0.30, P = 0.11	0.12, P = 0.18
ESVI (stress)	0.35, P = 0.06	0.30, P = 0.11	0.22, P = 0.23
SRS	−.03, P = 0.71	− 0.01, P = 0.89	− 0.04, P = 0.61
SSS	− 0.17, P = 0.41	− 0.21, P = 0.30	−0.07, P = 0.72

FDG, ^{18}F-fluorodeoxyglucose; *SUV*, standard uptake value; *LA*, left atrium; EF, ejection fraction; *EDVI*, end diastolic volume index; *ESVI*, end systolic volume index; *SRS*, summed stress score; *SSS*, summed stress core

Table 3.

Correlation of EKG parameters to metabolic parameters: Spearman rho correlation coefficients between EKG- and FDG-uptake values

	SUVmean	SUVmax	Blackout 50%
P axis (degree)	−0.078, P = 0.52	− 0.002, P = 0.98	0.07, P = 0.52
PR interval (ms)	−0.06, P = 0.58	− 0.16, P = 0.18	− 0.18, P = 0.11
P-duration Ave (ms)	0.11, P = 0.33	0.07, P = 0.58	0.009, P = 0.94
P wave deflection max (mv)	0.16, P = 0.18	0.187, P = 0.12	0.19, P = 0.11
P-wave terminal force (lVms)	0.29, P = 0.01	0.27, P = 0.02	0.18, P = 0.13

FDG, 18F-fluorodeoxyglucose*; SUV*, standard uptake value*; ms*, miliseconds*; mv*, millivolts; μV, microvolts